Australian Journal of Basic and Applied Sciences, 5(10): 1595-1604, 2011
ISSN 1991-8178

The Geochemical, Mineralogical and Characterization of Mineralization Zones In Quartz Diorite, Quartz Monzodiorite and Granite associations (Suite) of Tarik Dareh (Torbat-E Jam) area By Multispectral Data (Rs) and artificial Neural Networks (ann) Methods

[1]Razmara, M, [1]Yousefi, M and [2]Kavoosi, N.

[1]Department of geology, Ferdowsi university of Mashhad- Iran.
[2]Department of civil, Univercity Putra Malaysia

Abstract: The granitoid, quartz-diorite and quartz-monzodiorite associations of Tarik Dareh (Torbat-e Jam) and its related placers were examined by XRD, XRF, ICP-MS, RS and ANN methods. The Multispectral data (SAM method) was used for differentiating of lithological units and identification of minerals in the suite. The Envi software provided a means for classification of lithological units into 4 main groups. The geochemical studies showed the granitoid stock is peraluminous (A/CNK = 0.7-1.2) and high K calk alkaline ($Na_2O<K_2O$). The geochemical analysis and trace elements data showed I type, subduction zones and syn-collision VAG type for the granitoid stock in the area. The enrichment during differentiation of magma caused Au, Sb and W anomalous. The Artificial Neural Networks (ANN) method was developed to define favourability zones of occurrences of Au, W and Sb mineralizations and to assess the predictive power of the model. ANN results showed the most of Au anomaly (higher than 4 ppm) can be observed in inner and adjacent of quartzdiorite unit, anomaly of W (higher than 2.2 ppm) in monzogranite and syenogranite ones, but anomaly of Sb (higher than 1.2 ppm) in the quartzdiorite and monzogranite parts.

Key words: Artificial neural network, RS, Multispectral data, ICP-Ms, I type granitoid, Tarik Dareh, Envi.

Problems:
1- $Mg=Mg + Fe^{total}$ ratios
2- ASI
3- peraluminous
4- elimination of Na and Ca in ANN

INTRODUCTION

The Tarik Dareh suite which lies between 60˚ 47' to 60˚ 57' East longitudes and 35˚ 25' to 35˚ 30' North latitude is located in NE of Fariman ophiolitic melange. The granitoid stock is situated in the NE of Iran, 140 km southeast of Mashhad and 35 km NE of Torbat-e Jam city (Fig. 1). The intrusive stock has NW-SE trend. The area shows geological and structural complexity due to its location between three major structural zones of Kopeh Dagh, Binaloud and central Iranian blocks. As a result an important mineralization (e.g. gold and tungsten) in the area is originated from this complexity. Their lithological associations, intense deformation and strong re-mobilization cause ambiguity on the primary setting of the ore deposition.

ANN method has great potential in various fields of application such as pattern recognition, classification, identification, vision and control systems in solving complex problems (Oh and Lee??, 2010). An ANN is a ‘‘computational mechanism able to acquire, represent, and compute a mapping from one multivariate space of information to another, given a set of data representing that mapping’’ (Garrett, 1994). An ANN learns by adjusting the weights between the neurons in response to the errors between the actual output values and the target output values. At the end of this training phase, the neural network provides a model that should be able to predict a target value from a given input value (Lee, Ryu, and Kim, 2007). In this paper an attempt is made to understand the origin of gold mineralization in the Tarik Dareh stock from the geochemical and patrological relationships and prediction of probable mineralization in nearby areas by RS and ANN methods. In this study 568 samples were analyzed by ICP-Ms and 30 samples by XRF for characterization of specific elements and their concentrations.

Analytical Methods:

For detection and mapping of probable areas of gold, antimony and W deposits, the petrological and geochemical data were combined with RS analysis. By SAM (Spectral Angle Mapper) classification of the Landsat TM, a mineral map of the area was created by ENVI software.

Corresponding Author: Razmara, Department of geology, Ferdowsi university of Mashhad- Iran

The Tarik Dareh suite was investigated using RS, XRD, XRF, ICP-MS, and ANN methods. Major, trace and rare elements were measured in ACME Analytical Laboratories Ltd., Canada by XRF and inductively coupled plasma mass spectrometry (ICP-MS).

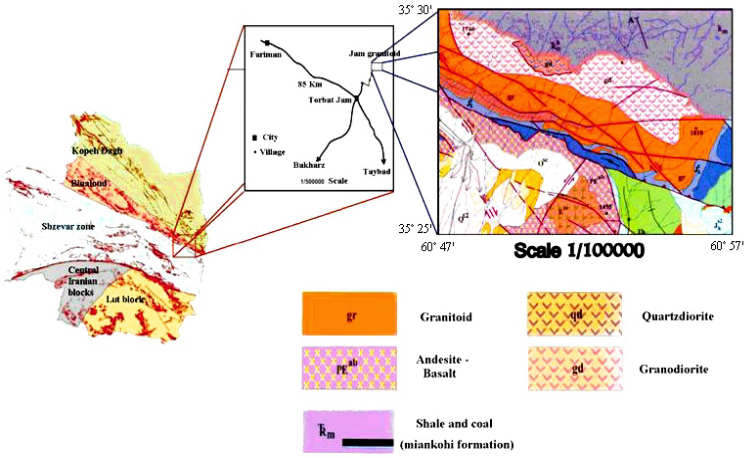

Fig. 1: The geological map of Tarik Dareh (Black valley) area.

RESULTS AND DISCUSSION

The Results of remote sensing (RS) and ETM$^+$ data, provided a means for classification of lithological units into 4 units. The granitoid body consists of monzogranite, syenogranite unites in the south but quartz-diorites and quartz-monzogranites in the north of the area. The petrographic and petrological data as well as remote sensing data have provided possible separation of lithological units with high accuracy (Fig. 2). A lot of minerals and rocks have characteristic spectral features in the range of 0.4–2.5 nm that allow their composition and relative abundance to be recognized and mapped from space. By using Multispectral images of Aster, it was possible for identification of major and minor minerals (Fig. 2). The SAM classification showed the best match at each pixel (Fig. 2). The results were in good agreement with mineralogical and petrographical studies of the units and XRD analysis. The granites show compositional changes and range from biotite + hornblende bearing monzogranite to syenogranite. The results of modal analysis are plotted on IUGS diagram which indicates calc-alkaline trend (Fig. 3). The exposure of intermediate rocks of the body in the northern part of the area and felsic one in the center can be represent of continous supply of magma without any disruption.

A field study to determine semi-quantitatively the distribution of mafic microgranular enclaves (MME) has been carried out in the area. mafic microgranular enclaves are present within the granitoid, making up <0.05% of the exposures. The majority of the enclaves are dark gray, fine grained and range in size from a few cm to about 0.50 m. MME enclaves are inferred to result from interactions between mafic rocks and felsic magmas.

The petrological, mineralogical and geochemical studies revealed a wide variety of alteration phenomena (e.g. potasic, sericitization and saussuritization alterations) in the area. This complexity is mainly displayed by mineralizations in veins and replacement along grain boundaries. In Jam granitoid, the alteration fabrics in the host rocks exhibit diversity above and below the main ore deposit zone. The most features are: (1) complex silica veins (2) authigenic K-feldspar and (3) mineralization of stibnite in the southern part of the stock.

The granitoid, quartz-diorite and quartz-monzodiorite associations of Tarik Dareh were formed by fractional crystallization of source magma. The associations vary in silica contents between 55.75 and 69.1% (Table 1), and are metaluminous to weakly peraluminous. The Tarik Dareh granitoid having average values of alumina (~14.50 wt% Al_2O_3), high values of potassium and sodium (~4.50 wt% K_2O; ~3 wt% Na_2O) and low values for calcium (~2.20 wt% CaO). Na_2O+K_2O vs SiO_2 (Irvin and Baragar, 1971) diagrams suggest that the bulk of the samples plot in the calc-alkaline (Fig. 4). The geochemical studies showed the granitoid stock is high K calk alkaline (Fig. 5). It can be concluded that the stock with Norian-Bajocian (upper Teriassic to middle Jurassic) age is metalumnous to weakly peraluminous (A/CNK=0.7-1.2) (Fig. 6). Excepting Al_2O_3, the major element oxides versus SiO_2 (Harker) diagrams display linear trends (Figs. 7). Fractionation of plagioclase and hornblende can explain the linear trends (Excepting Al_2O_3) of major oxides and trace elements in the Harker-type diagrams. Table 2 shows average values of selected trace elements for Tarik Dareh granitoid with respect to alteration and mineralisation. Variation diagrams of Zn vs silica (Kleins *et al*., 1982) and Zr vs silica (Newberry *et al*., 1990) diagrams indicating that the associations are I-type granitoids (Fig. 8).

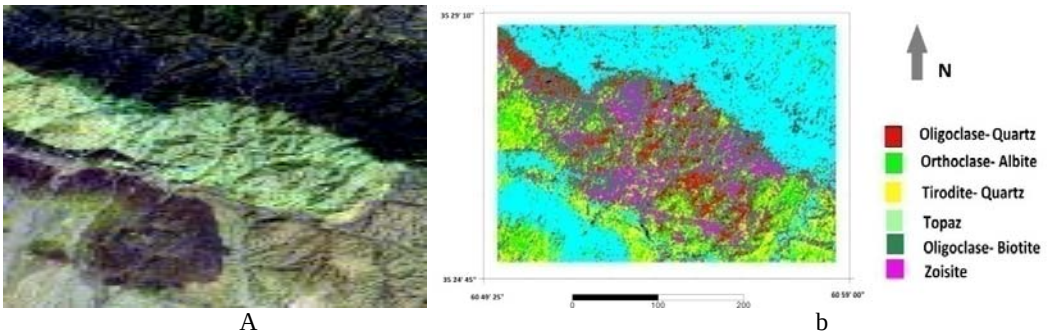

A b

Fig. 2: A) lithologic separation, b) presenting minerals by SAM method (ASTER).

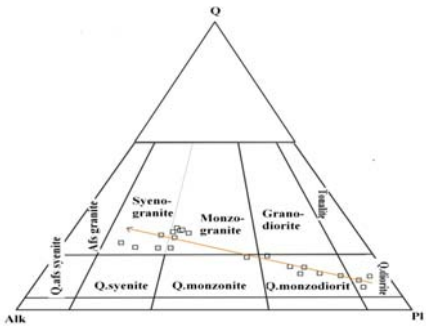

Fig. 3: Modal compositions of granitoid and quartz-diorite associations plotted on IUGS classification system and indicating trend of calc-alkaline (arrow).

Table 1: Selected chemical analyses of major oxides (wt %) in Tarik Dareh granitoid and comparisons with enclaves of granitoid from different localities in the area.

	Syenogranite			Monzogranite			Quartz monzodiorite			Quartz diorite			Enclave
	93TD	A1G	101TD	50TD	139TD	C1Gd	A1Qm	A4Sq	A3Qm	A2Qd	AH2To	A1Qd	A1E
SiO_2	69.1	66.33	68.6	65.73	66.68	64.63	58.23	60.61	56.66	58.56	56.99	55.75	52.11
Al_2O_3	14.33	15.32	14.93	15.32	14.34	16.29	14.41	14.79	14.87	14.38	14.42	13.9	16.82
Na_2O	3.08	2.79	2.84	3.78	3.11	3.03	2.77	2.67	2.54	2.83	2.86	2.13	3.15
MgO	1.46	1.5	1.32	1.9	2	1.51	3.15	3.1	3.64	2.83	4.03	4.66	4.28
K_2O	4.96	4.18	4.82	3.97	3.96	4.35	1.56	2.72	3.22	2.08	2.39	2.89	3.12
TiO_2	0.33	0.45	0.33	0.48	0.52	0.48	0.87	0.75	0.98	1.18	0.96	0.88	1.04
MnO	0.06	0.07	0.05	0.09	0.09	0.07	0.22	0.11	0.13	0.14	0.16	0.17	0.24
CaO	1.21	3.3	1.88	1.66	2.28	3.62	6.5	5.73	6.59	6.44	6.49	7.13	5.53
P_2O_5	0.09	0.12	0.09	0.11	0.15	0.12	0.53	0.3	0.36	0.56	0.38	0.28	0.4
Fe_2O_3	1.83	1.95	1.83	1.98	2.02	1.98	2.37	2.25	2.48	2.68	2.46	2.38	2.54
FeO	1.63	2.07	1.35	2.21	2.63	2.37	7.31	4.59	5.23	6.62	6.49	6.73	7.9
LOI	1	1.26	1	2.5	1.59	1.5	1.17	1.58	2.7	1.1	1.77	2.36	2.4
Total	99.08	99.34	99.04	99.73	99.37	99.95	99.09	99.2	99.4	99.4	99.4	99.26	99.53

Major elements determined by by XRF, ACME Analytical Laboratories Ltd., Canada

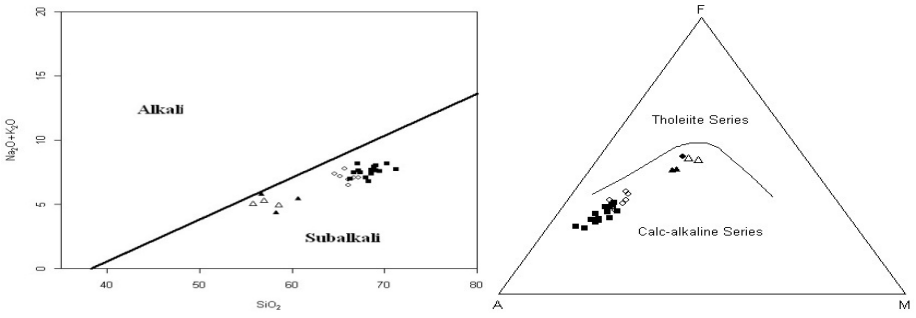

Fig. 4: Na_2O+K_2O vs SiO_2 and AFM diagram (Irvin & Baragar, 1971) suggest that the bulk of the samples plot in the subalkali and calc-alkaline fields.

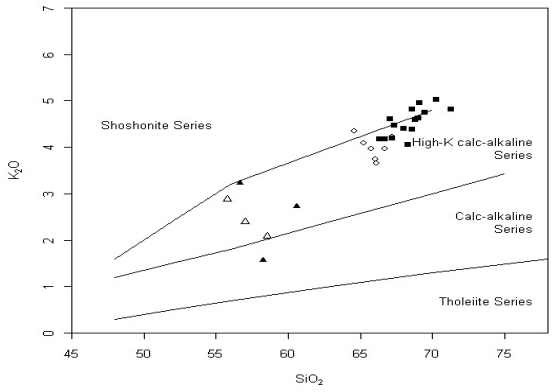

Fig. 5: K_2O vs SiO_2 diagram (Peccenillo and Taylor, 1976) suggest that the bulk of the samples plot in the high K calc-alkaline fields.

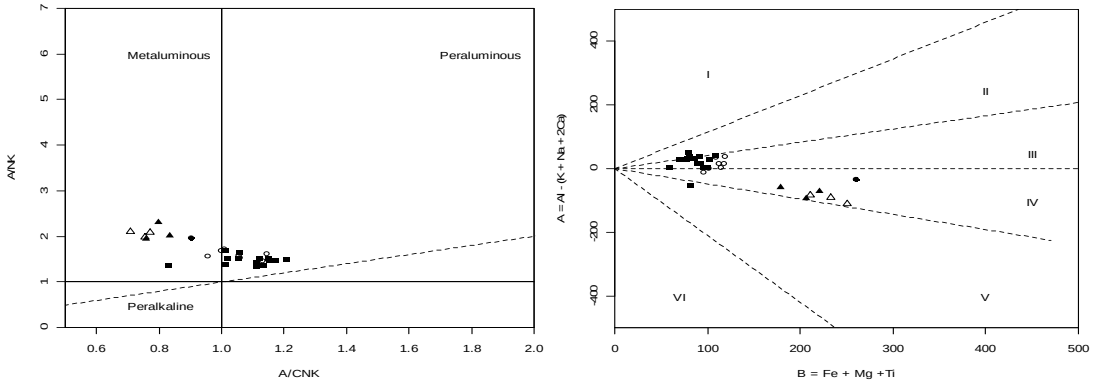

a b

Fig. 6: Major elements geochemistry: a) Debon & Le Fort (1983) diagram to determine Al index b) A/CNK vs. A/NK after Maniar and Piccoli (1989).

Table 2. Average values of selected trace elements (ppm) for Tarik Dareh granitoid with respect to alteration and mineralisation.

	19TD	21TD	29TD	31TD	32TD	33TD	34TD	35TD	55TD	59TD	61TD	102TD
Cu	3.79	24.42	4.22	3.58	4.82	4.83	11.37	10.06	5.25	4.01	3.95	4.66
Pb	17.7	13.44	12.2	13.6	13.98	13.15	13.41	19.78	14.32	14.11	17.94	15.98
Zn	27.2	36.2	31.4	29.8	30.3	36	30.6	34.2	29.5	25.6	30.7	32.1
Ni	5	6.7	4.7	5.5	5.5	6.5	5.7	5.6	5.4	5	5.3	5.1
Co	5.7	7.3	5.4	5.6	5.7	7.6	6.6	5.8	6	4.8	5.4	5.9
U	2.9	2.8	8.1	2.8	2.9	3.2	3.2	3.5	3.2	4.5	6.3	5.1
Th	24.6	26	25.4	20	20.8	24.9	26.7	23.2	24.4	31.1	35.3	30.9
Sr	342	262	103	257	287	264	271	252	252	270	269	263
V	36	53	42	44	43	53	46	40	39	37	45	45
Cr	17	25	19	19	19	20	19	23	16	17	19	15
Ba	831	1375	646	746	874	813	958	807	832	768	758	782
Zr	35.8	28.3	33.6	25.7	25	33	32.3	42.6	22.5	30.1	23.9	28.8
Sc	4.7	6.5	5.7	6	5.9	7.4	6	5.8	5.9	4.5	5.6	6.8
Y	20	20.6	18.7	17.5	18.4	21.2	19	19.1	19.5	18.8	22.6	22.9
Ce	125.8	101.4	86.75	81.95	81.74	99.98	98.71	90.62	99.85	89.09	123.3	91.32
Rb	164.2	134.5	149.5	156.3	143.2	148.2	151.4	157.9	141.6	124.9	113.5	125.9
Ta	1.5	1.3	1.4	1.5	1.3	1.5	1.2	1.3	1.3	1.6	1.7	1.7
Nb	22.24	25.49	23.93	24.08	23.07	27.56	24.24	23.18	24.86	23.46	26.3	28.19
Cs	3.7	2.9	3.4	5.4	4	4.2	4.3	4.6	4.9	4.6	5.6	6.7
Ga	15.69	15.92	13.75	14.77	14.71	16.71	14.6	13.96	14.64	14.16	14.31	14.87

Trace elements determined by ICP-MS, ACME Analytical Laboratories Ltd., Canada.

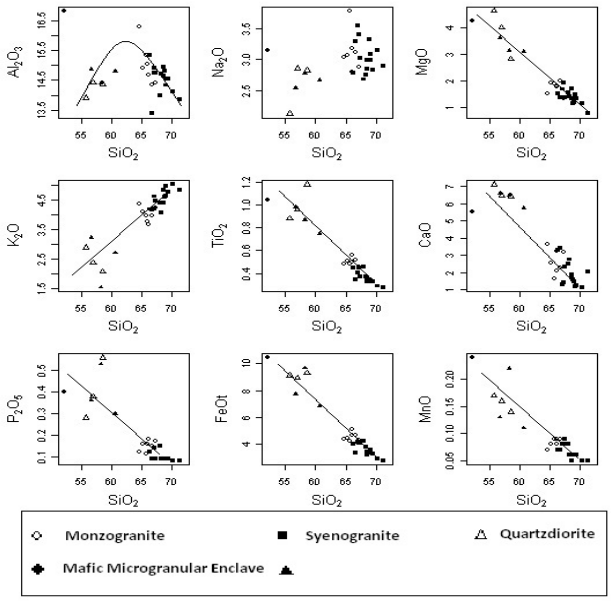

Fig. 7: Variation diagrams of major elements vs silica (Harker Diagrams).

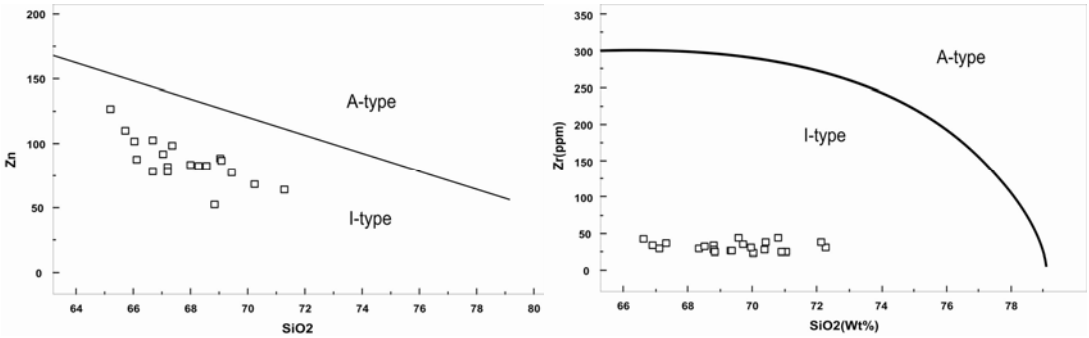

Fig. 8: Variation diagrams of Zn vs silica (Kleins et,al., 1982) and Zr vs silica (Newberry et,al., 1990) diagrams indicating that these are I-type granitoids.

The geochemical study of REE elements showed enrichment of LREE in compare of MREE and HREE and depleted in Eu (Table 3). These evidences indicated the importance of hornblende and plagioclase differentiation during the evolution of the granitoid in the area. The associations behave homogeneously on the MORB normalized REE plots with fairly flat HREE from Gd to Lu but negative Eu and Tm anomalies (Fig. 9). The result of XRF and ICP-MS in Harker diagrams showed effect of differentiation process combined with contamination. A detailed study of MME enclaves, A/CNK ranges less than 1.2, a negative changes in CaO and P_2O_5 versus SiO_2, the ratio of Fe_2O_3/FeO higher than 0.4, the major and trace elements diagrams, the behavior of trace elements, abundance of LILE elements such as Th, U, Rb, La, K and Pb, depletion of HFSE elements and comparison of multi-element (spider) diagrams, which normalized based on MORB (Fig. 10), all of the them indicate that the Tarik Dareh intrusion is a highly evolved I-type granite originating from the lower crust. The geochemistry of major and trace elements showed syn-collisional granite area which is in good agreement with VAG, CAG and KCG types.

Table 3. Representative analyses of REE elements of quartz diorite and granites based on (ppm) from average samples area.

	19TD	20TD	21TD	29TD	31TD	32TD	33TD	34TD	35TD	55TD	59TD	61TD	63TD
La	61.8	46	52.4	45	42.1	43.4	50.2	54.3	47.3	52.9	50.1	69.1	45.6
Nd	39.1	31.3	35.9	30.8	28.9	29.1	33.8	35.1	31.9	33.2	29.8	42	30.4
Sm	4.8	4.6	5.2	4.9	3.9	4.3	4.9	4.6	4.4	4.8	4.4	5.8	4.4
Eu	0.8	0.7	0.9	0.7	0.6	0.6	0.7	0.6	0.8	0.7	0.6	0.5	0.6
Gd	3.7	3.6	4.9	4.2	3.5	3.3	4	3.7	4	4	3.3	3.5	3.2
Tb	0.6	0.5	0.7	0.6	0.5	0.5	0.5	0.5	0.5	0.6	0.5	0.6	0.5

Dy	3.4	3.4	4	3.6	2.9	3	4	3.2	3.6	3.8	3.2	4.2	3.8
Yb	2.4	2.1	2.2	2.3	2.1	1.9	2.2	2	2.1	2	2.1	2.5	2.1
Lu	0.3	0.3	0.3	0.3	0.3	0.3	0.3	0.3	0.3	0.3	0.3	0.4	0.3

REE analysis determined by ICP-MS, ACME Analytical Laboratories Ltd., Canada.

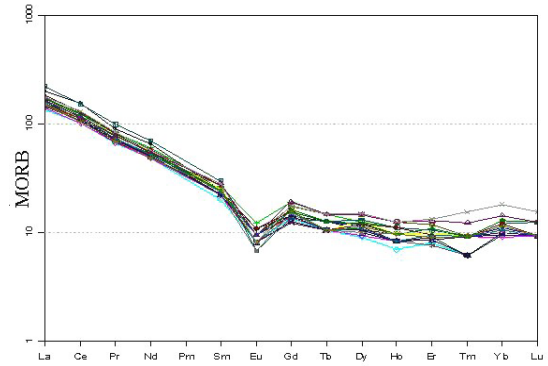

Fig. 9: REE elements normalized to MORB in quartz-diorite, quartz-monzodiorite and granites of Tarik Dareh.

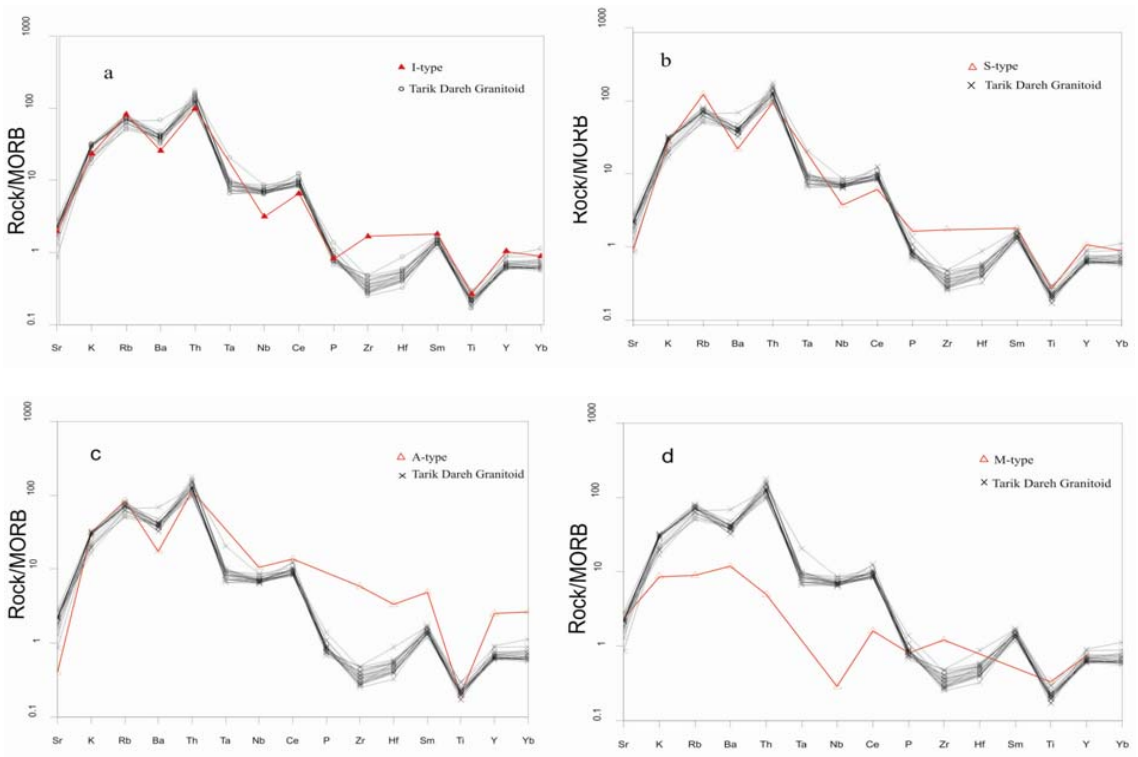

Fig. 10: Trace elements normalized to MORB in quartz-diorite, quartz-monzodiorite and granites of Tarik Dareh.

Four distinct stages of mineralization can be recognized throughout the area. The first stage is manifested during differentiation of primary magma and enrichment of magmatic fluids. The second phase occurred following uplift of the magma. This magma was particularly gas-rich which led to the generation of hot fluids. At depth these fluids precipitated pyrite with minor inclusions of stibnite and, rarely, gold. In the third stage, reduction in pressure (and the release of S and As) leading to the generation of sulfidation and the precipitation of arsenopyrite. The final stage was accompanied by alteration phenomena by hot fluids which caused leaching and silicification in the granitoid stock. Shallow-level deposits are typically characterized by gold associated with arsenic and antimony and locally elevated base metals, whereas deeper systems commonly contain abundant bismuth, tungsten and arsenic (Baker, 2005).

It is possible to predict which granites have the potential to be mineralised and there are several important parameters which can provide clues to the mineral potential (White *et al*., 1991). The Artificial Neural Networks (ANN) method was developed to define favourability zones of occurrences of Au, W and Sb mineralizations and to assess the efficiency and the predictive power of the model. Figure 11 shows the predicted and actual values for Au, Sb and W elements in the area. On the basis of experiments and modeling, an important objective was to obtain an ANN model that could make reliable prediction on the percentage of gold (Fig. 12), antimony (Fig. 13) and tungsten (Fig. 14) in the area. The validation data were: a) 560 Chemical analysis (by ICP-MS and XRF methods), b) 40 observations, c) The previous map from IUGS (1:100000 scale), d) compare the result with the other analysis.

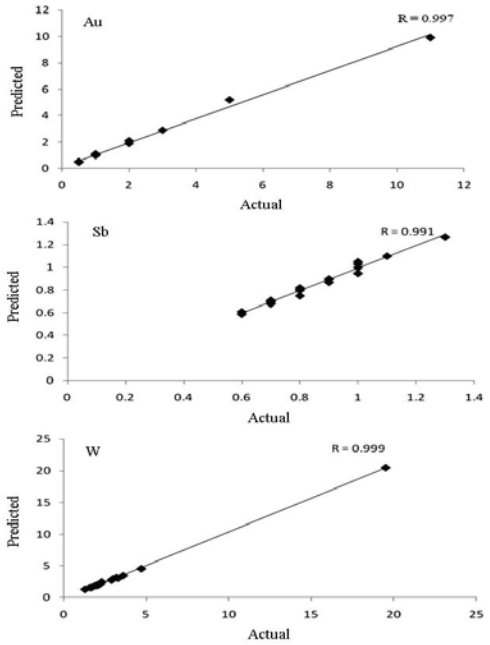

Fig. 11: The predicted and actual values for Au, Sb and W elements in quartz-diorite, quartz-monzodiorite and granites of Tarik Dareh.

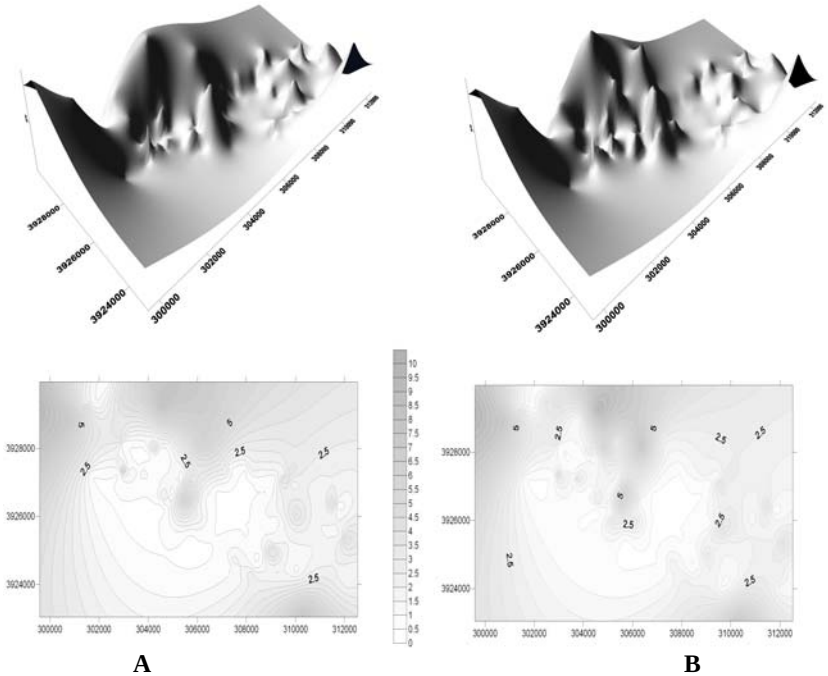

Fig. 12: The isograde map for gold. A) Actual data, B) predicted data.

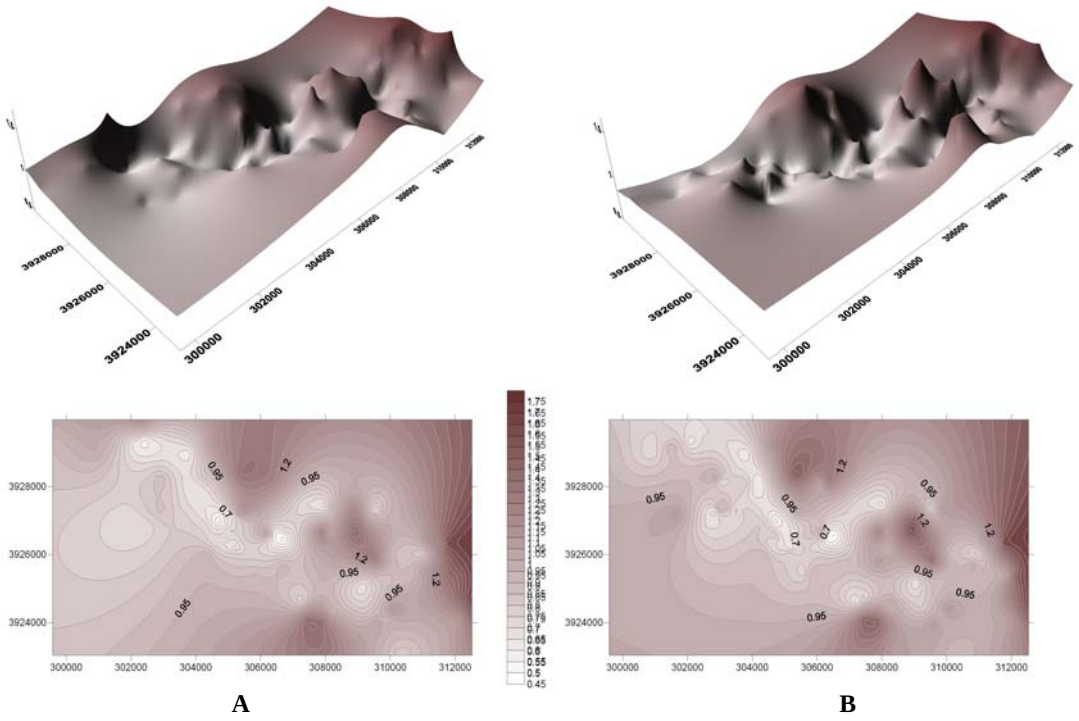

Fig. 13: The isograde map for antimony. A) Actual data, B) predicted data.

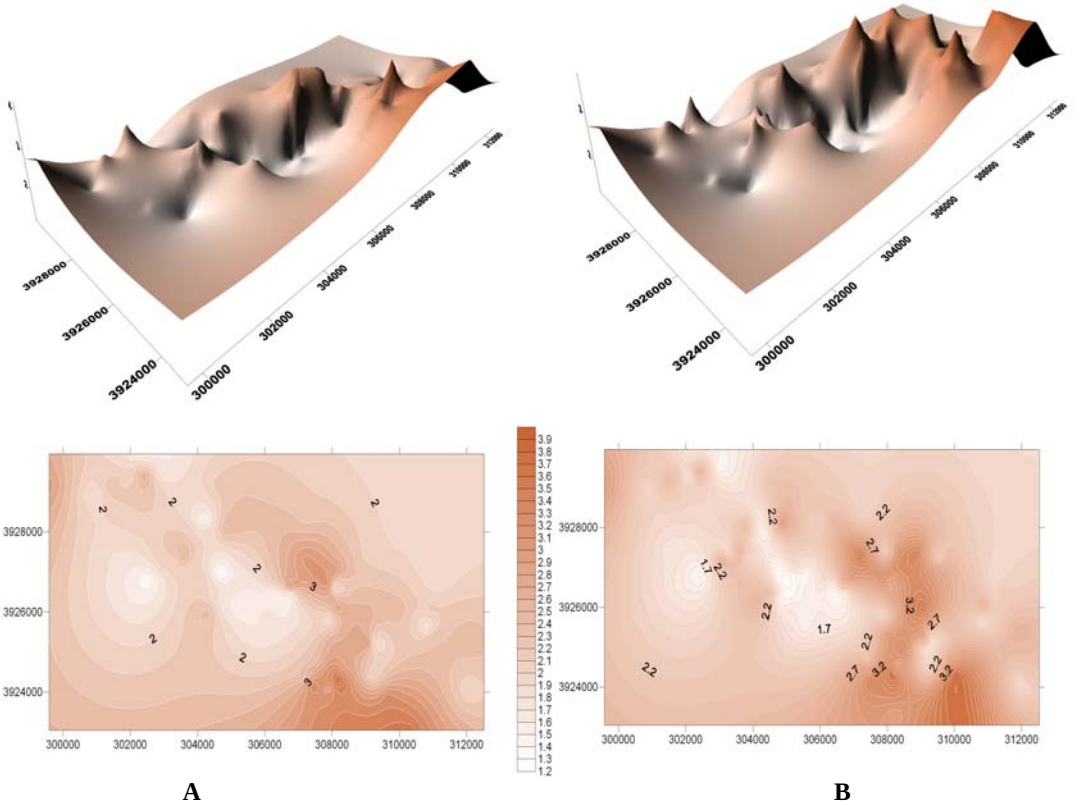

Fig. 14: The isograde map for tungsten. A) Actual data, B) predicted data

Conclusion:

The present study leads to the following conclusions:

- The major mineralized rock type in the area is granites, quartzmonzodiorite and quartzdiorite, which contains variable amounts of gold. The data allow us to subdivide the stock into four blocks. The complex ranges from depleted syenogranite and monzogranite to Au-bearing altered quartzdiorite.
- The geochemical data from major and REE elements indicated that the granitoids of the area are I type one.
- The results of modal analysis indicate a calc-alkaline trend and high potasic type with good agreement with AFM, Taylor and Peccenillo (1976) diagrams.
- The spider diagrams of REE elements showed that simultaneous differentiation of plagioclase, alkali feldspar and hornblende is a major factor in the magma transformation in the area.
- This study showed that the application of sophisticated RS and ANN method can raise the accuracy and effectiveness of mineralization quantitative prediction and evaluation. A better understanding of the geology in a region can be resulted by using remote sensing images. By analyzing of RS data we can select objects on the ground before fieldwork is performed.
- The geochemical analysis and trace elements data showed I type, subduction zones and syn-collision VAG type for the granitoid stock in the area. The enrichment during differentiation of magma caused Au, Sb and W anomalous.

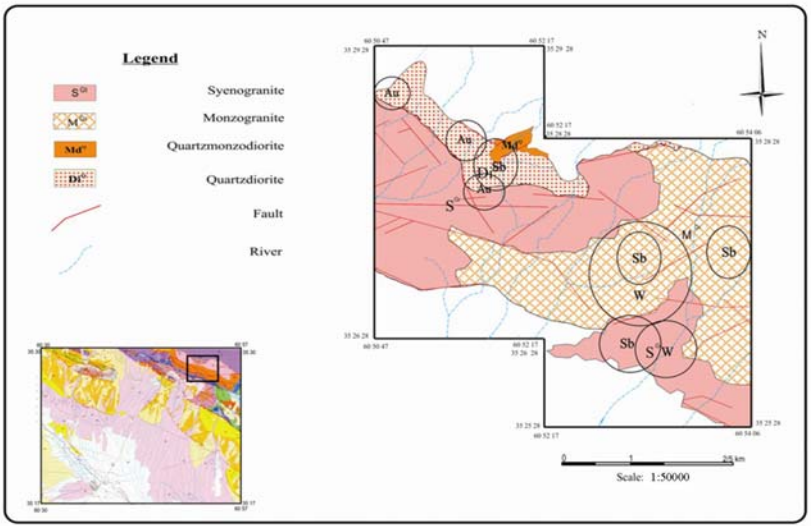

Fig. 15: The geological map and predicted mineralization potential by ANN method in Tarik Dareh area.

ACKNOWLEDGEMENTS

This work was supported by the Ministry of industry and mining of IR of Iran. The authors thank Mr Abbasnia for XRF and ICP-MS analyses.

REFERENCES

Alavi, N.M., 1989. Geology map 1:100000 Torbat-e jam, Geological survey of Iran.

Barth, M., S. Foley, and I. Horn, 2001. Partial melting in Archean subduction zones: constraints from experimentally determined trace element partition coefficients between eclogitic minerals and tonalitic melts under upper mantle conditions. Department of Earth and Planetary Sciences, Harvard University, 20 Oxford Street, Cambridge, MA 02138, USA.

Boardman J.W. and F.A. Kruse, 1994. Automated spectral analysis: A geologic example using AVIRIS data, north Grapevine Mountains, Nevada: in Proceedings, Tenth Thematic Conference on Geologic Remote Sensing, Environmental Research Institute of Michigan, Ann Arbor, MI, p: I-407-I-418.

Chappell, B.J. and A.J.R. White, 1974. "Two Contrasting Granite Types". Pac. Geol., 8: 173-174.

Chappell, B.W. and A.J.R. White, 1992. I-and S-type granites in the Lachlan Fold Belt. Transaction of the Royal Society of Edinburgh: Earth Science 83: 1-26.

Chappell, B.W. and A.J.R. White, 2001. Two contrasting granite type: 25 years later. Australian Journal of Earth Science, 48: 489-499.

Condie, K.C., 1989. Geochemical changes in basalts and andesites across the Archean-Proterozoic boundary: identification and significance. Lithos. 23: 1-18.

Garrett, J., 1994. Where and why artificial neural networks are applicable in civil engineering: J. Comput. Civil Eng., v. 8, p: 129-130.

Hassoun, M.H., 1995. Fundamentals of Artificial Neural Networks. MIT Press, Cambridge, MA.

Kuster, D. and U. Harms, 1998. Post-collisional potassic granitoids from the southern and northwestern parts of the Late Neoprotrozoic East African Orogen: a review. Lithos., 45: 177-195.

Lee, S., J.H. Ryu and I.S. Kim, 2007. Landslide susceptibility analysis and its verification using likelihood ratio, logistic regression, and artificial neural network models: case study of Youngin, Korea: Landslide, v. 4, p. 327-338.

Macias, C., M.K. Sen and P.L. Stoffa, 2000. Artificial neural networks for parameterestmation in geophysics: Geophys. Prospeting,48, 21-47.

Maier, H.R. and G.C. Dandy, 2000. Application of artificial neural networks to forecasting of surface water quality variables: Issues, applications and challenges. In: Govindaraju, R.S. and Rao, A.R. (Eds). Artificial neural networks in hydrology. Pp: 287-309.

Maniar, P.D. and P.M. Piccoli, 1989. Tectonic discrimination of granitoids. *Geological Society of America Bulletin*, 101: 635-643.

Marcello, E., J.B. Almedia, Moacir, C. Macambira, Elma, Oliveira, 2007. Geochemistry and zircon geochronology of the I-type high-K calc-alkaline and S-type granitoid rocks from southeastern Roraima, Brazil: Orosirian collisional magmatism evidence (1.97–1.96 Ga) in central portion of Guyana Shield, Geological Survey of Brazil.

Nykanen, V., 2008. Radial basis functional link nets used as a prospectivity mapping tool for orogenic gold deposits within the Central Lapland Greenstone Belt, Northern Fennoscandian Shield: Nat. Resour. Res., v. 17, p. 29-47.

Oh, H.J. and S. Lee, 2010. Application of Artificial Neural Network for Gold–Silver Deposits Potential Mapping: A Case Study of Korea. Natural Resources Research, Vol. 19, No. 2.

Rollinson. H., 1993. Using Geochemical Data: Evaluation, Presentation, Interpretation. Singapore, Longman, p: 352.

Rummelhart, D.E., G.E. Hinton and R.J. Williams, 1986. Learning internal representation by back propagating errors: Nature, 332: 533-536.

Strobl1, R.O. and F. Forte, 2007. Artificial neural network exploration of the influential factors in drainage network derivation. Hydrological processes., 21: 2965-2978.

Taylor, S.R. and S.M. McLennan, 1985. The Continental Crust: Its Composition and Evolution. Blackwell, Oxford, p. 312.

Thuy, N.T.B., M. Satir, W. Siebel, T. Vennemann, T.V. Long, 2004. Geochemical and isotopic constraints on the petrogenesis of granitoids from the Dalat zone, southern Vietnam. J. Asian Earth Sci., 23: 467-482.

White, A.J.R., D. Wyborn and B.W. Chappell, 1991. A granite classification for the economic geologist. *Geological Society of Australia, Abstracts*, 29: 57.

Winter, J. D., 2001. An Introduction to Igneous and Metamorphic Petrology. Prentice Hall, New Jersey, p: 697.

Wu, F.Y., B.M. Jahn and S.A. Wilde, 2003. Highly fractionated I-type granites in NE China, I: geochronology and petrogenesis. Lithos., 66: 241-273.